O. H. Pakarinen, A. S. Foster, M. Paajanen, T. Kalinainen, J. Katainen, I. Makkonen, J. Lahtinen, and R. M. Nieminen, Towards an accurate description of the capillary force in nanoparticle-surface interactions, Modelling and Simulation in Materials Science and Engineering 13, 1175 (2005).

INSTITUTE OF PHYSICS PUBLISHING MODELLING AND SIMULATION IN MATERIALS SCIENCE AND ENGINEERING

Modelling Simul. Mater. Sci. Eng. **13** (2005) 1175–1186 doi:10.1088/0965-0393/13/7/012

Towards an accurate description of the capillary force in nanoparticle-surface interactions

O H Pakarinen, A S Foster, M Paajanen, T Kalinainen, J Katainen, I Makkonen, J Lahtinen and R M Nieminen

Laboratory of Physics, Helsinki University of Technology, PO Box 1100, 02015 HUT, Finland

Received 14 April 2005, in final form 30 August 2005
Published 20 September 2005
Online at stacks.iop.org/MSMSE/13/1175

Abstract

We present a method to numerically calculate the exact (non-circular) meniscus profile from the Kelvin equation, and compare the results of the obtained capillary force with different previous approximations and experiments. We show that a circular meniscus profile gives correct results in most cases. We also compare different models of pull-off behaviour and show that the often used approximation of humidity independent capillary force is viable for spherical particles above 1 μm radius, but below that there is a strong humidity dependence, as seen in experiments. At the same length scale the direct surface tension force component becomes important. We also discuss the vanishing of the capillary force at very low humidity, the effect of small initial separation between the particle and the surface and the effects of different particle shapes and contact angles on the capillary force. Finally, calculated results are compared with experimental measurements of the capillary force.

(Some figures in this article are in colour only in the electronic version)

1. Introduction

The increasing quality and reliability of methods available in surface science has allowed experiments to move ever closer to the real environments which they attempt to model. Of particular importance is the role of humidity, and the subsequent formation of water films, in biological processes, wetting, corrosion, etc [1]. A simple system, common in many applications, is a nanoscale particle interacting with a surface in a humid ambient (e.g. air). The nature of the interaction between the particle and surface is strongly modified by the water meniscus which forms between them [2]. This meniscus results in an additional *capillary force* increasing the particle's adhesion to the surface. The capillary force can easily be the dominant interaction in these systems; hence it is important to understand and model it accurately.

Recently, atomic force microscopy (AFM) has become the tool of choice in studies of the capillary force as it allows one to directly measure adhesive forces as a function of ambient conditions. AFM also offers great measurement flexibility since the tip shape and material can be varied and particles can also be glued to the tip apex. Previous AFM studies [3–8] have

demonstrated how sensitive the capillary force is to both ambient humidity and tip/particle hydrophobicity. The complex nature of the capillary force has paradoxically meant that it is usually studied with very simple models [2,9–15]. These continuum models have proved their usefulness in macroscopic measurements, where water can be treated as a continuum, and simple model systems allow easy comparison between theory and experiment. However, AFM has moved the measurements from the macroscopic world closer to the atomic length scale, and the limits of applicability of the continuum modelling need to be checked, as well as the effect of new shapes and sizes of the tools on the models. Lattice gas simulations which intrinsically include the water molecules have recently demonstrated that even for the simplest particle shapes at the nanoscale it is crucial to reproduce the humidity dependence of the capillary force [16]. In this paper we attempt to find the limits of continuum modelling and establish more generally the effects of system structure and environment.

As stated previously, the capillary force is caused by the condensation of ambient humidity forming a meniscus or a liquid capillary neck between a particle and a surface. This meniscus grows in size, until its surface curvature has decreased to a value where the rate of evaporation and condensation is in equilibrium with the ambient. The surface curvature of the meniscus determines the pressure inside the meniscus. The capillary force is often said to arise from the *pressure difference* between the inside and the outside of the meniscus. This can, however, be misleading, as the outside (ambient) pressure is not significant in most cases, but the force arises from a large, negative Laplace pressure caused by surface tension inside the meniscus, i.e. the surface tension forces the water molecules further apart from each other than they would naturally be. For example, at 50% relative humidity the Laplace pressure is about—9×10^7 Pa, —900 times the ambient pressure. This negative Laplace pressure pulls the particle and surface together, causing the *capillary pressure force*. There is also a direct surface tension component in the capillary force, as surface tension pulls the contact line of meniscus and the particle towards the contact line of meniscus and the surface. This force is called the *surface tension force*.

2. Methods

Previous studies of particle–surface interactions using phenomenological models generally assume that the particle is spherical, and also apply restrictions to the meniscus shape. These approximations will be discussed later, but first we will attempt to build a more general model of the capillary force. In order to model other types of particle shape, specifically the type of truncated cones used in most SFM experiments, we develop a model for any axially symmetric particle shape. We also make no assumptions for the meniscus profile, and calculate the exact meniscus profile (nodoid [13]) where in all points of the profile the total radius of curvature

$$r = \left(\frac{1}{r_1} + \frac{1}{r_2} \right)^{-1}, \tag{1}$$

is correct. Here r_2 is the positive radius of curvature around the centre axis of the system and r_1 is the vertical radius of curvature, negative for the usual, concave shaped meniscus [17] (see figure 1). In thermal equilibrium this radius is given by the Kelvin equation

$$r = \frac{\gamma \upsilon_0}{kT \ln p/p_s}, \tag{2}$$

where γ is the surface tension, υ_0 is the molecular volume of the liquid, k is the Boltzmann constant, T is the system temperature and p/p_s is the relative humidity. We calculate the profile by aligning small line elements—the first line element is placed to start from some point of the particle–surface, so that the angle between the tangent of the particle–surface and

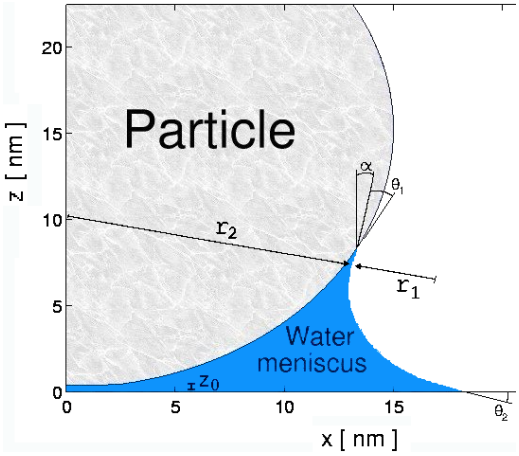

Figure 1. Schematic diagram showing the meniscus formed between a particle of radius R at a distance of z_0 from a surface at $z = 0$. r_1 is the vertical radius of curvature, r_2 is the symmetry radius of curvature, θ_1 is the particle contact angle and θ_2 is the surface contact angle.

the line element is the given contact angle θ_1. The end point of the element now determines the symmetry curvature radius r_2 (from the rotation axis) at the corresponding height, and the vertical radius of curvature r_1 can be obtained from equations (1) and (2). The next line element needs to be aligned so that the curvature matches the required r_1. The radius of curvature can be calculated as

$$r_1 = \frac{[1 + (\mathrm{d}x/\mathrm{d}z)^2]^{3/2}}{\mathrm{d}^2x/\mathrm{d}z^2}, \tag{3}$$

from which we can solve the direction of the next line element:

$$\mathrm{d}^2x = \frac{\mathrm{d}z^2[1 + (\mathrm{d}x/\mathrm{d}z)^2]^{3/2}}{r_1}. \tag{4}$$

This alignment of line elements is continued until the profile touches the surface. The angle between the surface and the last line element is calculated, and if this does not match the desired contact angle θ_2, a new starting point is estimated, and the profile is updated until the desired contact angle is obtained.

After the profile is calculated, we also know the xy-projection of the area of the particle on which the negative Laplace pressure Δp focuses. For an area projection of A_{xy} with the Laplace pressure defined as

$$\Delta p = \gamma\left(\frac{1}{r_1} + \frac{1}{r_2}\right) = \frac{kT \ln p/p_s}{\upsilon_0}, \tag{5}$$

the capillary pressure force (F_{cp}) is given by

$$F_{\mathrm{cp}} = A_{xy}\frac{kT \ln p/p_s}{\upsilon_0}. \tag{6}$$

To calculate the surface tension force, we calculate the perimeter l of the contact between meniscus and particle, and the surface tension force (F_{st}) is obtained from

$$F_{\mathrm{st}} = l \cdot \gamma \cos\alpha, \tag{7}$$

where $\gamma \cos\alpha$ is the vertical component of the surface tension (see figure 1). In all calculations presented here, values for water at 20 °C were used, $\gamma = 72.8\,\mathrm{mJ\,m^{-2}}$ and $\gamma\upsilon_0/kT = 0.54\,\mathrm{nm}$ [2].

3. Validity of the approximations

In this section we consider two of the most general approximations used to calculate the capillary force, and compare them with our more exact model to define the range of their validity. In the examples we use spherical particle shapes, zero particle–surface separation $z_0 = 0$ and zero contact angles, unless otherwise stated.

3.1. Large spherical particles

One of the most common approximations applied is to consider the interaction of macroscopic size spherical particles with a surface, where r_2 is much larger than r_1. Now the projected area, A_{xy}, is πr_c^2, where r_c is the radius of the contact line at the top of the meniscus. From equation (6), the capillary pressure force is

$$F_{\mathrm{cp}} = \pi r_c^2 \frac{kT \ln p/p_s}{\upsilon_0}. \tag{8}$$

For large spheres (radius R) $r_2 \gg r_1$, $\Delta p = \gamma/r_1$, and

$$r_c^2 + (R - r_1(\cos\theta_1 + \cos\theta_2))^2 = R^2$$
$$\Rightarrow r_c^2 \approx R^2 - R^2 + 2Rr_1(\cos\theta_1 + \cos\theta_2) = 2Rr_1(\cos\theta_1 + \cos\theta_2)$$

and we obtain the capillary pressure force

$$F_{\mathrm{cp}} = \frac{\gamma\pi r_c^2}{r_1} = 2\gamma\pi\frac{Rr_1(\cos\theta_1 + \cos\theta_2)}{r_1}$$
$$= 2\gamma\pi R(\cos\theta_1 + \cos\theta_2). \tag{9}$$

If we further assume that the contact angles, θ_1 and θ_2, are the same and independent of humidity, and that the surface tension force component is small enough to be neglected, one obtains the most common formula or *standard approximation* [2,13,18] for the capillary force:

$$F_c = 4\pi\gamma R\cos\theta. \tag{10}$$

Under these assumptions the capillary force is actually humidity independent. This has been shown experimentally [18] to hold for some large particles, but several experiments [3,4] have also shown strong humidity dependence of the particle–surface adhesion force for smaller particles. Our calculations for the capillary pressure force show (see figure 2) that the standard approximation really is valid for spheres of 1 μm radius, but below that a strong humidity dependence arises. This is particularly important when considering modelling of SFM experiments, as tips usually have a radius in the range 10–100 nm.

It is also often assumed [2] that the surface tension force is negligible compared with the capillary pressure force for all but the highest humidities. However, the results in figure 3 show that this also has a strong dependence on particle size. The surface tension force is negligible with 1 μm radius spherical particles, but for particles with a 15 nm radius it can be a larger component of the total capillary force than the capillary pressure force.

3.2. Circular profile approximation

Generally it is assumed that the capillary force can be calculated using a circular meniscus side profile, i.e. r_1 is the same for all points of the profile. For large particles it is clear that because $r_2 \gg |r_1|$, r_1 is almost the same at every point, but for small objects this is not the case, as r_1 is of about the same magnitude as r_2. Our calculations do not make that approximation,

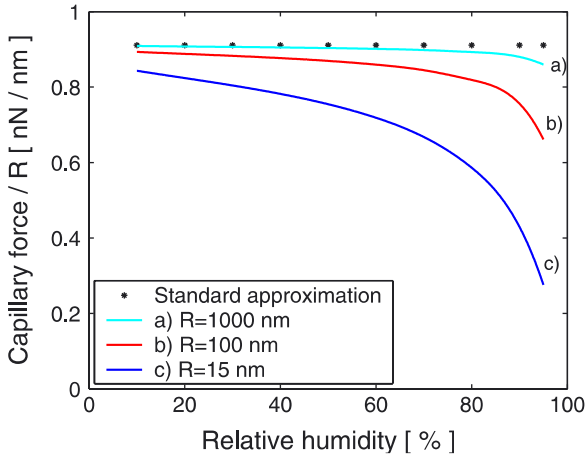

Figure 2. Applicability of the standard model of capillary force for different particle sizes, showing the humidity dependence of the capillary pressure force for spherical particles with zero particle–surface separation (z_0).

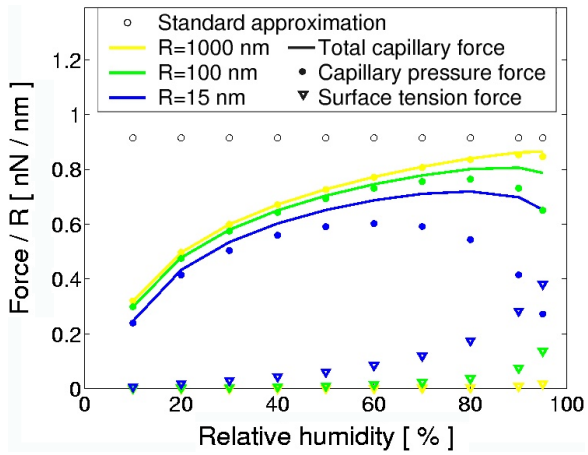

Figure 3. Humidity dependence of the capillary force components at 3 Å particle–surface separation.

but the correct r_1 is calculated from the Kelvin equation (equation 2). Our results, shown in figure 4, for spheres of different radii show, however, that this approximation is justified in the size range where continuum modelling can be used.

4. Factors influencing humidity dependence of capillary force

4.1. Particle shape

The particle shapes also have a strong effect on the humidity dependence of the capillary force. Often the experiments are done by assuming—and striving towards—a perfect spherical geometry of the particle. This is sensible, as small deviations from the shape do not result in large changes in forces. If one, however, tries to model the capillary force between an SFM

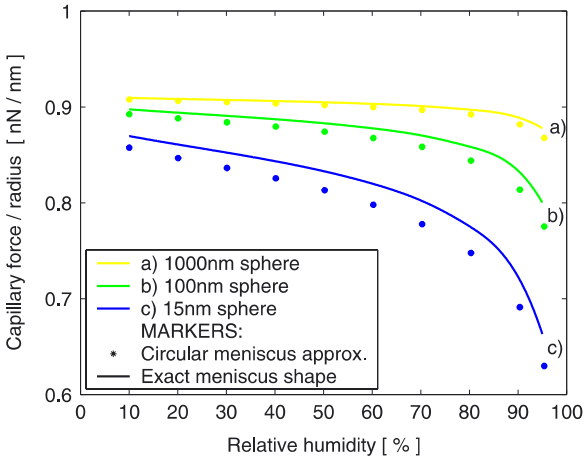

Figure 4. Capillary forces calculated with circular profile approximation, compared to exact profile. For 1000 nm radius sphere the match is more or less perfect, for 100 nm sphere there is an error of about 1%, and for 15 nm sphere the error is about 2–3%.

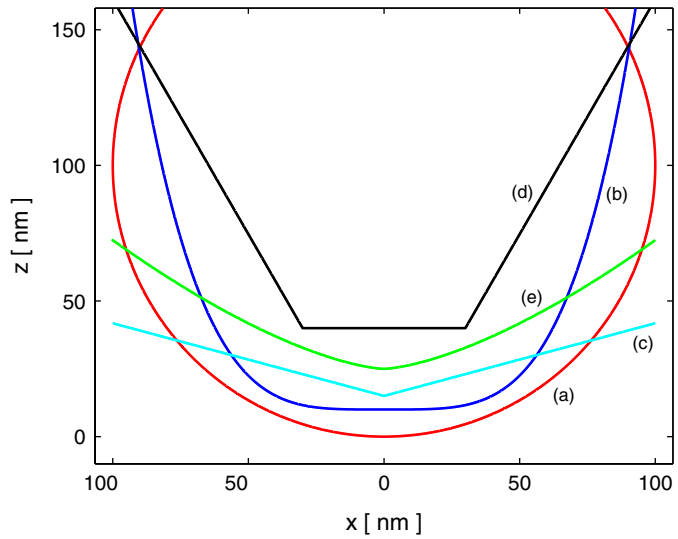

Figure 5. Tip shapes in humidity dependence calculations: (*a*) sphere ($R = 100$ nm); (*b*) $z = k_b x^4 (k_b = 2 \times 10^{21})$; (*c*) cone (cone angle $\beta = 15^\circ$); (*d*) truncated cone ($R = 30$ nm and cone angle, $\beta = 60^\circ$); (*e*) $z = k_e x^{3/2} (k_e = 1500)$.

tip and a surface by assuming conical or truncated conical tip shapes, for example, much more caution is needed.

Figure 5 shows the profiles of the five different particles shapes considered. The truncated cone is formed by removing the apex of a cone, leaving a finite apex radius. Very sharp particle shapes, such as sharp cones, are not considered, as for these the capillary meniscus is very small, and use of continuum modelling is unjustified. Figure 6 shows the dependence of capillary force between these particles and a flat surface as a function of humidity. We can immediately see that the shape has a crucial effect on the magnitude and the humidity dependence of the force.

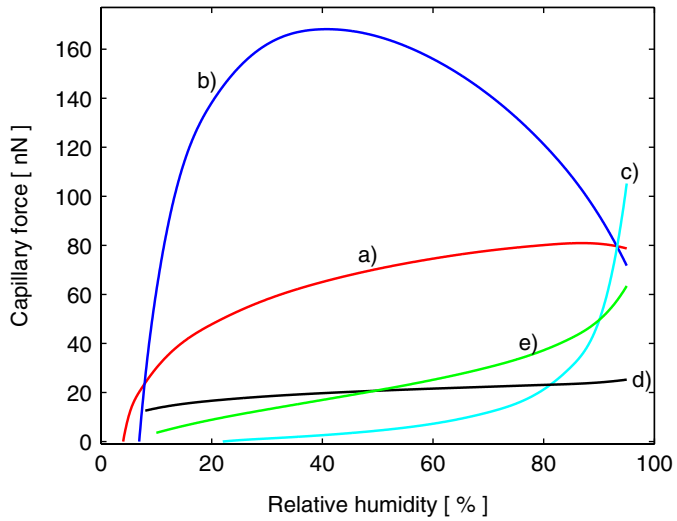

Figure 6. Effect of particle shape on humidity dependence of the capillary force for the particle profiles shown in figure 5. Particle–surface separation $z_0 = 3$ Å.

4.2. Separation between the particle and the surface

In the continuum model with zero separation z_0, a non-vanishing capillary force is predicted also for the limit $p/p_s \to 0$. This is obviously an unphysical result, as there is no longer any water to create the force. In reality there is a lower limit for $|r_1|$, because of the molecular (non-continuum) structure of water, of the order of diameter of a water molecule (≈3 Å). If the horizontal edge of the meniscus is formed by one or two water molecules, the curvature, in continuum terms, can no longer be defined, and also the pressure difference tends to zero.

In the case of z_0 greater than a few angstroms, the continuum model is valid, because it predicts formation of a meniscus only after the continuum approximation of the meniscus edge is valid. The question of space between the particle and the surface is very important also in another way—the calculated continuum capillary pressure force is determined by the area under the meniscus, and for blunt particles this can vary a lot, depending on how small a gap between the particle and the surface the water is thought to be able to fill. Figure 7 shows that both for a spherical and a blunt particle, the increasing separation induces a lower limit of humidity, below which a meniscus is not formed, and also changes the humidity where maximum force is obtained. For the blunt $z = kx^4$ particle the filling limit discussed above has been set to 4 Å. Therefore the maximum force is not obtained at contact, $z_0 = 0$, but at a separation above the filling limit. For both particle shapes the curves tend towards a common value at the highest humidities, because then the meniscus is over 10 nm in height, and small changes (of a few angstroms) in particle–surface separation do not have a large effect.

4.3. Contact angles

Hydrophilicity or hydrophobicity of the surface, i.e. the contact angles between the water meniscus and both the surface and the particle have an important role in capillary condensation, and they largely determine the shape of the meniscus, and therefore also the capillary force strength. Figure 8 shows some comparisons of the contact angle dependence of the capillary force for the standard approximation (equation (10)), and our exact profile method. For the

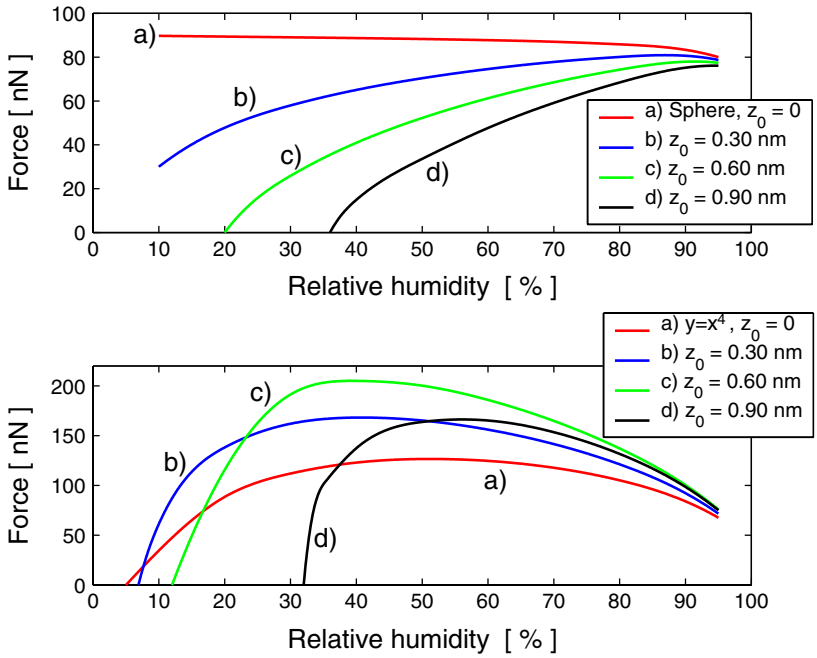

Figure 7. Effect of particle–surface separation on humidity dependence of the capillary force, for a spherical, $R = 100$ nm (above) and a blunt $z = kx^4$ (below) particle.

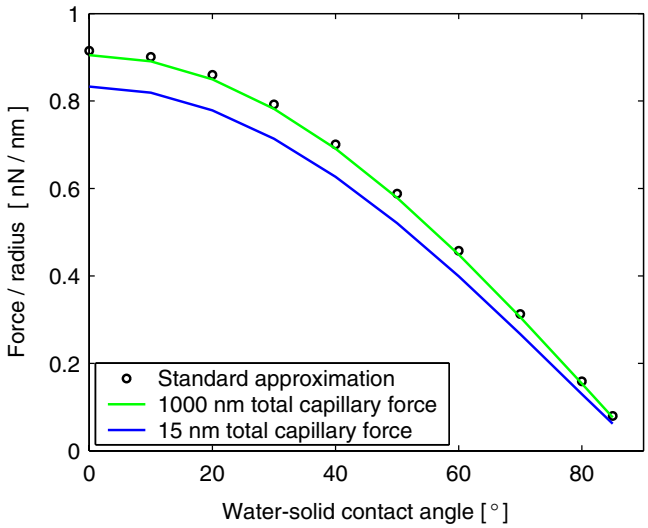

Figure 8. Contact angle dependence of the capillary force, for 1 μm and 15 nm radius spheres, at 50% humidity. For both particle sizes, the force is proportional to the cosine of the contact angles, as in standard approximation.

large 1 μm radius sphere the standard approximation describes the force well, and the surface tension component is small in all humidities. For a small 15 nm radius sphere the match is not so good, as already seen in figure 2, and at large contact angles the surface tension force rises above the capillary pressure component.

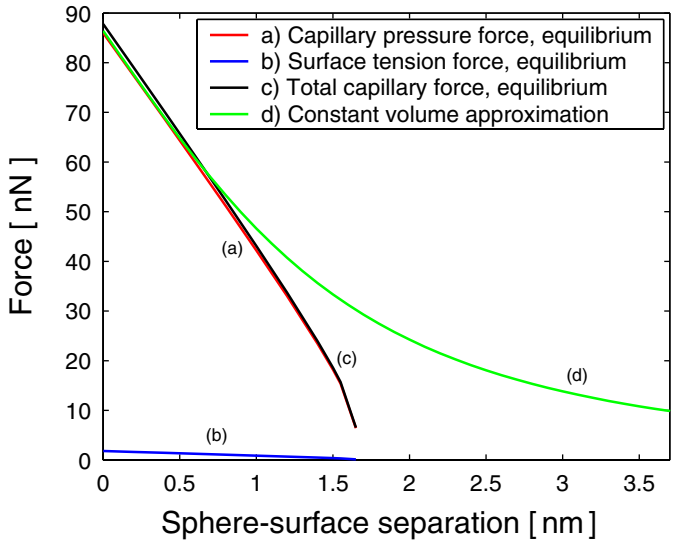

Figure 9. Capillary force versus particle–surface separation in pull-off. Results for a spherical particle of 100 nm radius, zero contact angles, 60% humidity.

5. Particle pull-off

Up to this point we have considered only methods for calculating the magnitude of the capillary force upon formation of the meniscus. However, many applications and also SFM, depend more critically on the force required to remove the particle from the surface—the *pull-off force*. When pulling the particle off the surface, the capillary force resists the pull-off until the meniscus breaks at some point. This force as a function of particle–surface separation can be modelled in two different ways—after the formation of the meniscus the volume of the meniscus can be approximated as constant [15], or the meniscus can be assumed to be in equilibrium with the surrounding atmosphere all the time during the pull-off [16], so that the meniscus volume decreases in pull-off. In figure 9 we use the exact profile method to show that these two approximations differ significantly in their results. The constant volume approximation predicts an attractive force for a spherical particle until 10 nm, whereas by staying in equilibrium all the time our calculations predict that the meniscus breaks already at 1.65 nm, in good agreement with previous results obtained with a lattice gas method [16]. The relaxation times in such a small system are definitely much shorter than any pull-off rate in SFM, etc. This is shown, for example, in a molecular dynamics study of formation of a meniscus of similar size [19], where about one million 5 fs time steps were needed, i.e. equilibrium was reached in about 5 ns. Therefore, the constant volume approximation usually is not applicable to nanometre sized menisci, but an equilibrium can be assumed.

6. Comparison with experiments

In order to test the model developed in this study, we also try to compare directly with the experimental measurements of the capillary force. In the first case we consider published experimental results [3], which demonstrated a strong humidity dependence of the capillary force for a Si_3N_4 AFM tip interacting with a hydrophilic silica (SiO_2) surface. The authors

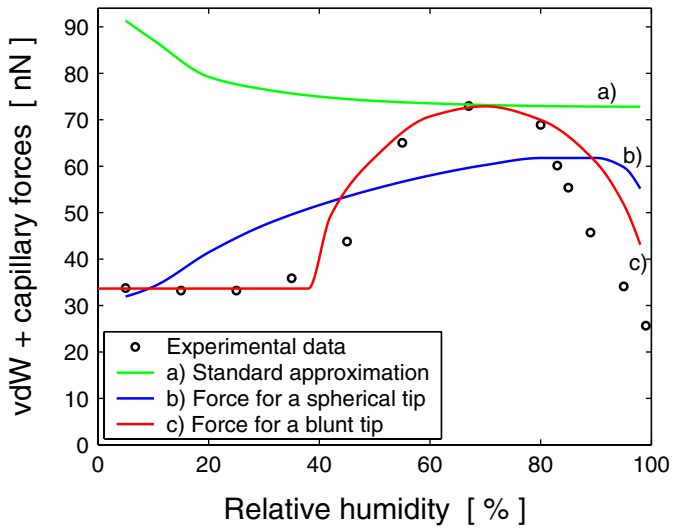

Figure 10. Capillary and van der Waals forces combined for different models. The van der Waals force is partially screened by the water meniscus. (*a*) Standard approximation, 100 nm sphere. (*b*) 100 nm sphere, $z_0 = 2.5$ Å. (*c*) $z = kx^3$, $k = 1.58 \times 10^{12}$, $z_0 = 8.0$ Å. For all calculations the contact angles were $\theta_1 = 60^\circ$ and $\theta_2 = 0^\circ$.

could only explain some features of the humidity dependence by assuming a spherical tip shape with a measured 100 nm radius, and suggested the deviation from a perfect shape as a reason for the mismatch. We can indeed show much better agreement with the experiment by assuming a blunter tip ($z = kx^3$, $k = 1.58 \times 10^{12}$, a shape between (*a*) and (*b*) in figure 5) and a larger effective separation (see figure 10). It must be noted that the larger separation, which does not match the separation used in the calculation of the van der Waals force, need not be the smallest physical separation between the particle and the surface, but just a parameter characterizing the shape of the particle at the height of the perimeter of the meniscus–particle contact.

Secondly, we performed a series of adhesion force experiments on a smooth (RMS roughness ≈3 Å) silica surface. Experiments were carried out with a Nanoscope III AFM with an atmospheric hood. The humidity was controlled with a self-made humidifier, adjusting flows of dry and humidified N_2 at a precision of 1.5% relative humidity. The tip was a Mikromasch single crystal silicon AFM tip. The cantilever was calibrated [20] and had a spring constant of $0.20\,\mathrm{N\,m^{-1}}$. All data points corresponded to a 10×10 matrix of measurements, with 100 nm separation between each measurement, and every data point was measured in a different part of the surface to avoid the wear of the surface. The measurements are well reproducible and have the same humidity dependence whether increasing or decreasing the humidity during collection of the measurement series.

Using our model with almost paraboloidal $z = kx^{1.82}$($k = 8.3 \times 10^{-4}$) tip and $z_0 = 2.07$ Å, we find a good agreement between simulation and experiment (see figure 11). The van der Waals force is calculated separately for every humidity, approximating the tip shape with a sphere of 35 nm radius, using smallest values of radii r_2 as the boundary for using water or air as a medium (which manifests as the Hamaker constant). In calculations both contact angles used are 61°, a value measured from the SiO_2 surface.

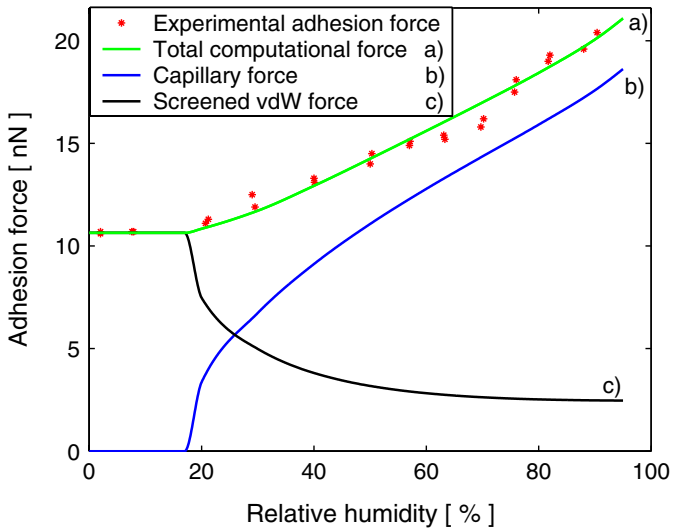

Figure 11. Capillary and van der Waals forces for a silicon AFM tip on SiO_2 surface. A paraboloidal tip shape fits the data well.

7. Discussion

In this paper we have considered in detail the approximations which are generally used to calculate the capillary force. Although we find that in many cases more simplistic approaches can be successful, when the size of the particle interacting with surface approaches the nanoscale many approximations become invalid. This is of particular importance when considering the capillary force in scanning force microscopy experiments, where the size of tip may be as small as 1–2 nm. Although more advanced atomistic-like methods [16] offer more complete simulations of capillary bridge formation, this study demonstrates that phenomenological modelling can still provide accurate simulations of the capillary force at a much reduced computational cost. In fact, a better approach is to use the lattice gas methods as a reference for parametrizing simpler models [21]. The real limit of phenomenological modelling is the point at which the water layer can no longer be considered to be a continuum, and each water molecule must be represented—a system where accuracy can only be achieved with advanced quantum mechanical methods [22].

We have shown that if the different shapes of the particle are taken into account it is possible to find very different humidity dependence of the capillary force, and hence better understand experimental results. This sensitive dependence of the capillary force on the particle shape also highlights the importance of observing or controlling this during experiments. The theoretical model has the freedom to simulate any particle shape, but this also means that a unique solution may not be found, and several possibilities may match the experimental results. Direct observation of the particle shape, or control of the shape during production would remove this element of uncertainty and increase the quality of the understanding provided by the simulations.

In order to provide a more complete demonstration of the validity of phenomenological models of the capillary force, the next step is to perform a series of AFM experiments with different tip shapes (known from imaging) and materials, and with both hydrophobic and hydrophilic surfaces, and compare them with computational results obtained by using the real

tip shapes and tip and surface parameters. Although this study has shown that the model can match the humidity dependence seen in two experimental examples, it is important to develop this success into a general understanding across a wide variety of systems.

Acknowledgments

This work was undertaken as part of the Academy of Finland Centre of Excellence programme 2000–2005, and the TEKES project SURFOX.

References

[1] Thiel P A and Madey T E 1987 *Surf. Sci. Rep.* **7** 211
[2] Israelachvili J N 1991 *Intermolecular and Surface Forces* (London: Academic)
[3] Xiao X and Qian L 2000 *Langmuir* **16** 8153
[4] Zitzler L, Herminghaus S and Mugele F 2002 *Phys. Rev.* B **66** 155436
[5] Xu L, Lio A, Hu J, Ogletree D F and Salmeron M 1998 *J. Phys. Chem.* B **102** 540
[6] Sedin D L and Rowlen K L 2000 *Anal. Chem.* **72** 2183
[7] He M, Blum A S, Aston D E, Buenviaje C and Overney R M 2001 *J. Chem. Phys.* **114** 1355
[8] Eastman T and Zhu D-M 1996 *Langmuir* **12** 2859–62
[9] Gao C, Dai P, Homola A and Weiss J 1998 *J. Tribology* **120** 358–68
[10] Gao C 1997 *Appl. Phys. Lett.* **71** 1801–3
[11] Marmur A 1993 *Langmuir* **9** 1922
[12] de Lazzer A, Dreyer M and Rath H J 1999 *Langmuir* **15** 4551
[13] Orr F M, Scriven L E and Rivas A P 1975 *J. Fluid Mech.* **67** 723–42
[14] Rabinovich Y I, Adler J J, Esayanur M S, Ata A, Singh R and Moudgil B M 2002 *Adv. Colloid Interface Sci.* **96** 213
[15] Stifter T, Marti O and Bhushan B 2000 *Phys. Rev.* B **62** 13667–73
[16] Jang J, Schatz G C and Ratner M A 2004 *J. Chem. Phys.* **120** 1157
[17] Adamson A W 1976 *Physical Chemistry of Surfaces* 3rd edn (New York, London: Wiley)
[18] McFarlane J S and Tabor D 1950 *Proc. R. Soc. Lond. Ser.* A **202** 224
[19] Seveno D and De Coninck J 2004 *Langmuir* **20** 737
[20] Sader J E, James W M and Mulvaney P 2000 *Rev. Sci. Instrum.* **70** 3967
[21] Jang J, Schatz G C and Ratner M A 2004 *Phys. Rev. Lett.* **92** 085504
[22] Xu X and Goddard W A 2004 *J. Phys. Chem.* A **108** 2305